AIAA JOURNAL
Vol. 36, No. 4, April 1998

Experimental Study of an Unsteady Separating Boundary Layer

E. A. Lurie,* D. P. Keenan,† and J. E. Kerwin‡
Massachusetts Institute of Technology, Cambridge, Massachusetts 02139

The objective of this research is to map the flowfield around the trailing edge of a hydrofoil subject to transverse gust loading, to provide guidance for the formulation of an appropriate Kutta condition for inviscid solution methods. The hydrofoil is equipped with a trailing edge that incurs boundary-layer separation over the last few percent of the chord. Mean and unsteady velocity profiles are presented for the Reynolds number of 3.8×10^6 and reduced frequency of 3.6. The location of the separation point in steady flow is identified, and the region of the separation trajectory in unsteady flow is seen. The magnitude and phase of the unsteady circulation and lift are found and compared to those values predicted by linearized methods.

Nomenclature

C = hydrofoil chord
C_D = drag coefficient, $D/\frac{1}{2}\rho U_0^2 C$
C_L = lift coefficient, $L/\frac{1}{2}\rho U_0^2 C$
D = drag force
h = distance normal to hydrofoil surface
k = reduced frequency, $\omega C/2U_0$
L = lift force
$\boldsymbol{n}$ = unit normal vector
p = pressure
Q = traveling wave speed
$\boldsymbol{q}$ = velocity vector
Re = Reynolds number based on hydrofoil chord, $U_0 C/\nu$
T = period of oscillation
t = time
U_0 = nominal freestream speed
u = velocity component in tangential direction (in boundary layer) and velocity component in streamwise direction (in wake)
u_e = mean tangential velocity at edge of shear layer (in boundary layer) and mean streamwise velocity at edge of shear layer (in wake)
w = velocity component in vertical direction
x = distance from leading edge in the streamwise direction
z = distance in vertical direction; 0 at trailing edge
Γ = airfoil circulation
γ = vortex sheet strength
Θ = phase
θ = momentum thickness

$$\int_0^\infty \frac{u}{u_e}\left(1-\frac{u}{u_e}\right)\mathrm{d}z$$

ν = kinematic viscosity
ρ = density
ω = radian frequency

Subscripts

TE = trailing edge value
0 = time-mean value
1 = first harmonic value

Received Feb. 19, 1997; revision received Nov. 18, 1997; accepted for publication Nov. 23, 1997.

*Graduate Student, Department of Ocean Engineering; currently Associate Research Engineer, United Technologies Research Center, 411 Silver Lane, M/S 129-17, East Hartford, CT 06108. Member AIAA.
†Research Engineer and Lecturer, Department of Ocean Engineering; currently Consultant, Coldstream Research, Sandwich, MA 02563.
‡Professor of Naval Architecture, Department of Ocean Engineering.

Introduction

MARINE propeller design methods are based on numerical techniques that assume smooth inviscid flow over the blade surface. This assumption is not valid for modern blade sections, which are intentionally built to develop boundary-layer separation over the last few percent of the chord. The small region of separation reduces the possibility of self-excited vibrations caused by the interaction of trailing-edge vortex shedding with structural vibration of the blade, commonly known as singing. In addition to the assumption of nonseparating flow, unsteady inviscid methods must assume a Kutta condition to render a unique solution; a common implementation models the wake as a thin sheet emanating from a zero-pressure-difference trailing edge and traveling at freestream speed. In this study the primary objective is to provide guidance for the formulation of an appropriate Kutta condition for unsteady inviscid methods, where small regions of separation are present. Although it has recently become feasible to perform Navier–Stokes computations of unsteady viscous flow around two-dimensional hydrofoil sections,[1–3] these simulations are able to reproduce the unsteady shear layer behavior only in a qualitative manner and do not accurately capture the time-mean separation and, hence, the time-mean forces. For design purposes, inviscid methods are still the true workhorses. A second objective of this study is to provide data for validation of unsteady viscous computations.[§]

Numerous experiments have been performed to explore the nature of the unsteady Kutta condition, and yet no consistent pattern emerges. In part this is due to the various definitions of the Kutta condition, as each experiment is designed to serve a particular definition. Some experiments have tried to examine the Kutta condition by reconstructing the streamlines in the immediate vicinity of the trailing edge. Large streamline curvature is an indication that severe normal pressure gradients exist and the boundary-layer approximation no longer holds. Experiments by Ho and Chen,[4] Poling and Telionis,[5,6] and Liu et al.[7] present contradictory conclusions for the range of reduced frequencies over which such a Kutta condition is valid. Attempts to replace the reduced frequency with a dynamic similarity parameter, which includes the amplitude of oscillation, do not clarify the results.[8]

Other unsteady airfoil experiments have tried to examine the Kutta condition by measuring the surface pressure as close to the trailing edge as possible. Commerford and Carta,[9] Satyanarayana and Davis,[10] Fleeter,[11] and Lorber and Covert[12] all found for a wide range of reduced frequencies and oscillation amplitudes that difference pressure amplitudes tended to zero at the trailing edge but that, over much of the chord, the measured amplitude and phase differed significantly from the classical theory. Although unsteady loading

[§]All data collected over the course of the experiment, along with additional documentation, may be found at http:\\ptun.mit.edu\ffx\Welcome.html.

variations in the trailing-edge region may not affect the magnitude of the unsteady lift, the unsteady moment may be significantly altered. Also, the poor agreement of the measured phase lag of pressure with theoretical analyses has significant implications for studies of turbomachinery flutter and noise generation.

Experimental Setup

Experiments were conducted at the Massachusetts Institute of Technology Variable Pressure Water Tunnel. A description of the facility is given by Lurie.[8] Instantaneous velocities are measured using a laser Doppler velocimeter (LDV). A two-component system is used for horizontal and vertical velocity measurements in the freestream and wake areas. A single-component fiber-optic probe is used for shear layer measurements: The probe is rotated in its mount so that it measures velocity tangent to the hydrofoil surface. Both laser systems sit on a table and traverse system that can be moved in 0.01-mm steps.

The experimental layout with relevant dimensions is given in Fig. 1. A large stationary hydrofoil is mounted on the tunnel centerline. Upstream are two small hydrofoils (flappers) symmetrically offset from the centerline. The flappers are linked to rotate in phase about midchord. A shaft encoder records the angular position of the flappers in their cycle. The upstream hydrofoils' shed vortex sheets create a vertical or transverse sinusoidal gust along the tunnel centerline. A summary of the geometries of the test hydrofoil and upstream flapping hydrofoils is given in Table 1. A description of the development of the test hydrofoil can be found in Ref. 13. A description of the development of the unsteady experiment apparatus can be found in Ref. 14. Relevant test parameters are shown in Table 2.

For steady flow measurements, the flappers are feathered to zero angle of attack and locked in position. Velocity data were obtained by averaging 250 laser events for each data point. To characterize the inflow conditions, velocity and pressure data were taken in three nested control volumes surrounding the stationary test hydrofoil. These traverses were between the wakes of the flapping foils and the test foil and along vertical faces upstream and downstream of the test foil. Steady boundary-layer velocity data were taken in eight chordwise locations on the suction side and seven chordwise locations on the pressure side. The table on which the LDV sits moved in 0.025-mm steps along a line extending normal to the foil surface, thus preserving the local coordinate system. Streamwise and vertical velocity data were collected in the wake along vertical traverses at five x/C locations.

Table 1 Summary of hydrofoil geometries

Test hydrofoil	
Chord length	457.2 mm
Thickness form	NACA 16
Maximum thickness/chord	8.84%
Camberline	NACA $a = 0.8$
Maximum camber/chord	2.576%
Boundary-layer trips	$x/C = 0.105$
Angle of attack	1.2 deg
Flappers	
Chord length	76.2 mm
Thickness form	NACA 0025
Angle of attack	±6 deg

Table 2 Summary of experimental conditions

Nominal freestream velocity U_0	6.28 m/s
Water temperature	25.6°C
Reynolds number Re	3.8×10^6
Reduced frequency k	3.6

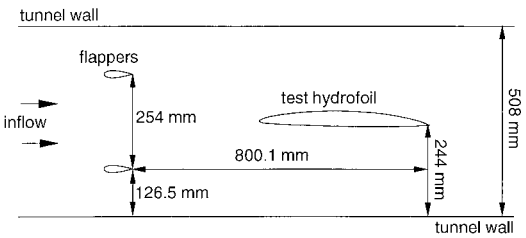

Fig. 1 Experimental setup.

Unsteady velocity data were obtained by phase averaging 88 batches of 512 bursts of data. A single harmonic cycle was divided into 180 bins, each containing approximately 250 laser events. To characterize the inflow conditions, unsteady velocity and time-mean pressure data were taken in three nested control volumes surrounding the stationary test foil. These traverses were in the same location as the steady traverses. Also, the upstream and downstream vertical faces of the middle of the three boxes were extended outward through the vortex sheets shed by the upstream flapping foils. Fourier analysis of the streamwise and vertical velocity measured upstream of the test hydrofoil leading edge indicates that the inflow is characterized as a time-mean upwash plus a small, relative to freestream, vertical gust:

$$u/U_0 = 1.00 \qquad \text{at} \qquad x = -0.26C, \quad z = 0.033C \tag{1}$$

$$w/U_0 = 0.0544 + 0.218\sin(\omega t - 79.56\,\text{deg})$$

$$\text{at} \qquad x = -0.26C, \quad z = 0.033C \tag{2}$$

Note that time $t = 0$ corresponds to flappers at zero angle of attack; t increasing corresponds to the flappers moving initially to positive angles, and so forth, through the cycle.

Unsteady boundary-layer tangential velocity data were taken at six chordwise locations on the suction side and two chordwise locations on the pressure side. For each of these traverses, the single-component fiber-optic probe was rotated so that the beam intersection lay tangent to the foil surface to measure tangential velocity. Unsteady streamwise and vertical velocity data were collected in the wake along vertical traverses at five x/C locations.

Experimental Results and Analysis

The experimental results are presented in terms of mean tangential velocity profiles in the boundary layer, ensemble-averaged boundary-layer profiles, mean streamwise and vertical velocity profiles in the near wake, and Fourier amplitudes and phase-lag distributions for these quantities. The experimental uncertainties were calculated in accordance with Ref. 15. Details of the error analysis may be found in Ref. 16. The uncertainties assuming a 95% confidence level are shown in Table 3.

A harmonic analysis was performed for each component of velocity at each (x, z) location where data were collected. The following convention was used:

$$f(x, z, t) = a_0(x, z) + \sum_{n=1}^{20} a_n(x, z)\sin[n\omega t + \Theta_n(x, z)] \tag{3}$$

Time-Mean Velocity

The graphs of steady and time-averaged tangential velocity vs distance normalized by chord length are shown in Fig. 2. As expected for small amplitude unsteadiness, the two data sets are nearly identical. Inspection of the suction-side data indicates that in steady flow there is boundary-layer separation between $x/C = 0.97$ and $x/C = 0.99$. Also, the edge velocities at suction side $x/C = 0.97$ and pressure side $x/C = 1.0$ are equal to less than 0.3%, so that within the boundary-layer approximation these are the separation points. The graphs of steady and time-averaged streamwise and vertical velocity vs distance normalized by chord length in the near wake are shown in Fig. 3. Again, the two data sets are nearly identical: The unsteady wake contracts at the same rate as the steady wake. In a small region just surrounding the trailing edge, occlusion of the LDV beams prevents streamwise velocity measurement.

Periodic Component of Boundary-Layer Velocity

Figures 4 and 5 show the amplitude and phase of the fundamental harmonic of tangential velocity in the boundary layer vs distance normalized on mean momentum thickness. The amplitude

Table 3 Experimental uncertainties

Streamwise velocity	0.15 m/s	2.4% U_0
Vertical velocity	0.10 m/s	1.6% U_0
Tangential velocity	0.26 m/s	4.1% U_0
Location in harmonic cycle	2 deg	0.56%

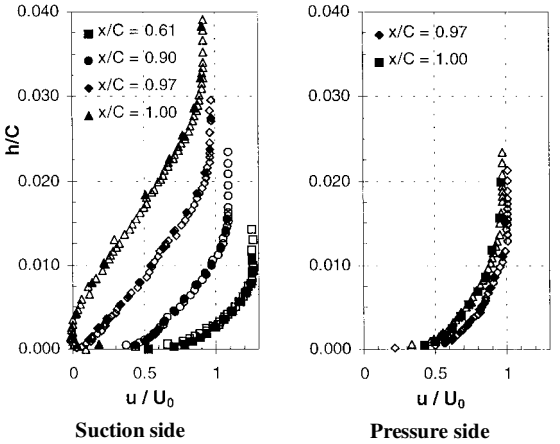

Fig. 2 Steady and time-mean unsteady tangential velocity: open symbols, steady data, and closed symbols, time-mean unsteady data.

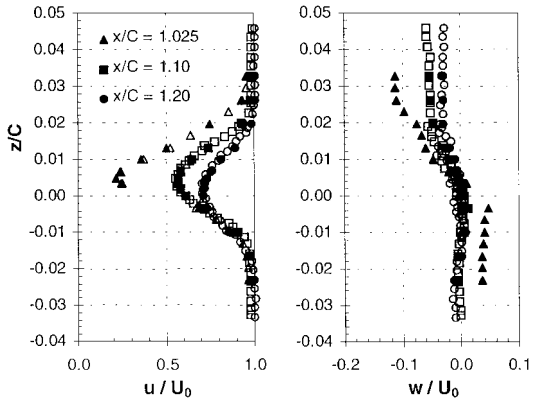

Fig. 3 Steady and time-mean unsteady velocity, near wake: open symbols, steady data, and closed symbols, time-mean unsteady data.

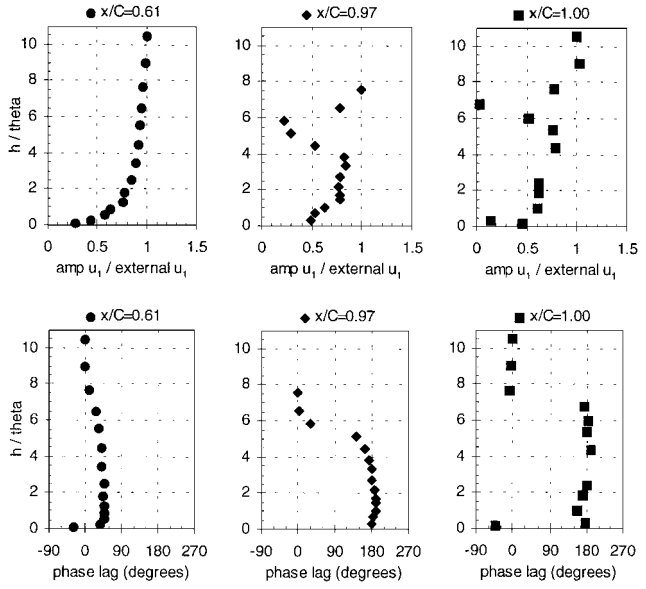

Fig. 4 Amplitude and phase lag of fundamental harmonic of tangential velocity with respect to edge values, suction side.

is normalized by the amplitude of the same harmonic of the external flow, and the phase is presented as lag of the fundamental harmonic with respect to the phase of the same harmonic of the external flow. The most striking feature is the dip or local reduction in amplitude at approximately 6–6.5 momentum thicknesses beginning with $x/C = 0.90$ on the suction side. This behavior appears to be developing on the pressure side as well. It is not known why the location of minimum amplitude is fixed at normal distance 6–6.5 momentum thicknesses. From the phase data it is seen that, at the height of minimum unsteady amplitude, there is a very large phase

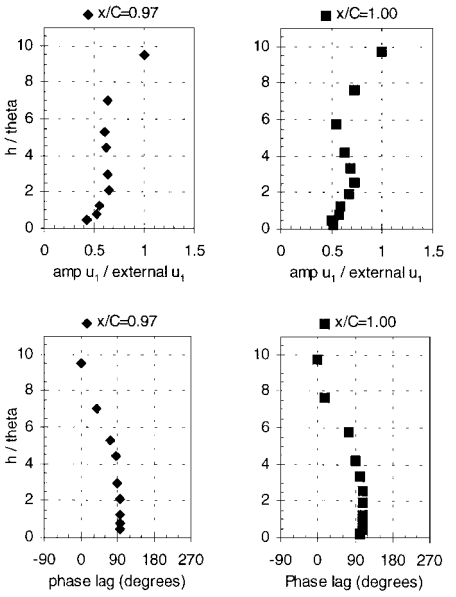

Fig. 5 Amplitude and phase lag of fundamental harmonic of tangential velocity with respect to edge values, pressure side.

shift with respect to the external flow. Near the suction-side trailing edge, this phase shift is close to 180 deg.

The variation of amplitude and phase through the boundary layer is not unexpected after considering how the freestream forcing interacts with the boundary-layer velocity. The edge velocity can be written as

$$u_e(x, t) = u_{e0}(x) + u_{e1}(x) \exp\{i\omega[t - (x/Q)]\} \tag{4}$$

If Eq. (4) is substituted into the pressure gradient terms of the boundary-layer momentum equation, then to first order the time-dependent forcing is

$$\left[u_{e0}\frac{\partial u_{e1}}{\partial x} + u_{e1}\frac{\partial u_{e0}}{\partial x} + i\omega u_{e1}\left(1 - \frac{u_{e0}}{Q}\right)\right]\exp\left[i\omega\left(t - \frac{x}{Q}\right)\right] \tag{5}$$

Approaching the trailing edge on the suction side, the wave speed $Q \approx u_{e0}$, so that the imaginary term in Eq. (5) is small compared with the spatial gradient terms, which are negative. Thus, the oscillating pressure gradient acting on the blade surface lags the freestream by almost 180 deg. On the pressure side, however, the spatial gradients are near zero and the wave speed $Q < u_{e0}$, so that the oscillating pressure gradient lags the freestream by 90 deg. Two regions are set up within the boundary layer, with minimum velocity amplitude and large phase shifting at the interface. Similar behavior has also been reported by Patel[17] and Kenison.[18]

Another way to visualize the effect of unsteadiness on the boundary-layer profiles is to consider the ensemble-averaged profile. The ensemble-averaged profiles for suction side $x/C = 0.97$ and $x/C = 0.99$ are shown in Fig. 6. Note the change in normalization of the ordinate from mean momentum thickness to chord length; this change was made to make the data more readable. The height of minimum unsteady amplitude is evident.

One can identify possible candidates for unsteady separation profiles by examining the shape of the ensemble-averaged profiles. Moore, Rott, and Sears (see Ref. 19) independently proposed as conditions for unsteady separation the simultaneous vanishing of the shear and the velocity at a point within the boundary layer and in a frame of reference moving with the separation point; in other words, moving at speed u_{sep},

$$u = 0, \qquad \frac{\partial u}{\partial h} = 0 \tag{6}$$

Although it is necessary to know the speed of the separation point to locate exactly the separation trajectory, the general shape of the velocity profile at separation is evident: It must have an infinite slope at some height. Furthermore, for harmonic motions of the separation point, during that part of the cycle when the separation point

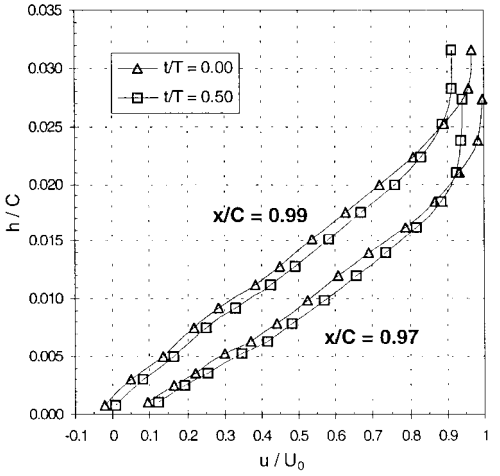

Fig. 6 Ensemble-averaged boundary-layer profiles, suction side.

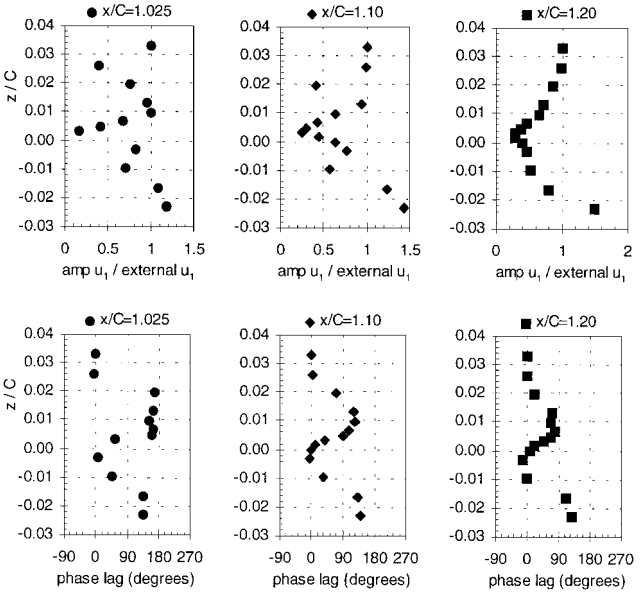

Fig. 7 Amplitude and phase lag of fundamental harmonic of streamwise velocity with respect to upper-edge values, near wake.

is moving upstream, some portion of the boundary-layer profile has negative velocity. In Fig. 6, neither profile has an infinite slope within the measured part of the boundary layer. Nonetheless, at $x/C = 0.97$ the profiles have all values of $u > 0$, whereas at $x/C = 0.99$ the profiles show $u < 0$ at the data point closest to the wall. Therefore, between these two chordwise locations lies the separation point at some height $h/C < 8 \times 10^{-4}$, the height of the data point closest to the wall. In physical space this is an approximately 9.1×0.4 mm area.

Periodic Component of Wake Velocity

The joining of the unsteady parts of the suction- and pressure-side boundary layers in the near wake is shown next. The amplitude and phase of the fundamental harmonic of the streamwise velocity in the wake vs vertical distance normalized on chord length is shown in Fig. 7. The amplitude is normalized by the amplitude of the same harmonic of the external flow at the upper surface, and the phase is presented as lag of the fundamental harmonic with respect to the phase of the same harmonic of the external flow at the upper surface. At every streamwise location but the farthest downstream, the unsteady velocity minima from both suction- and pressure-side boundary layers is evident: for example, at $x/C = 1.025$, $z/C = -0.01$, and $z/C = 0.025$. By $x/C = 1.20$ these local amplitude minima have been mixed out. But the phase shifting inside the shear layer is still present and diminishes as the flow moves downstream. The external flow has an almost constant 130-deg phase difference between the upper and lower wake surfaces at all chordwise locations.

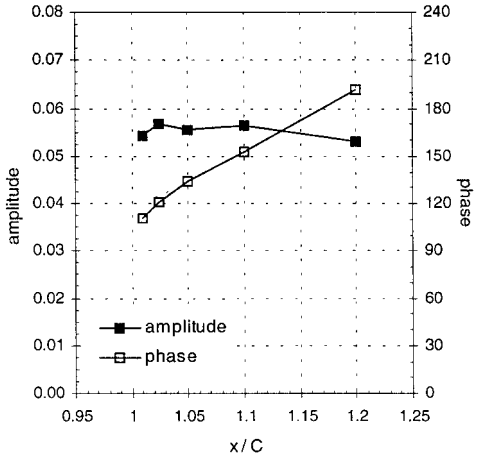

Fig. 8 Magnitude and phase of wake vortex sheet.

Although not shown, the unsteady part of the vertical velocity is almost completely damped out; the largest fundamental harmonic amplitude of w for all five wake traverses is $0.008U_0$.

If we imagine, as in classical thin-airfoil theory, that the wake consists of a thin vortex sheet located on the x axis of strength $\gamma(x,t) = u^+(x,t) - u^-(x,t)$, where $u^{\pm}(x,t)$ are the streamwise velocities measured at the upper and lower edges of the wake, then as seen in Fig. 8 this vortex sheet can be represented by

$$\frac{\gamma(x,t)}{U_0} = \text{const} \times \exp\left[\omega\left(t - \frac{x - x_{\text{TE}}}{Q}\right)\right] \tag{7}$$

In other words, despite the large transverse variations in velocity amplitude and phase, the simple approximation of a thin vortex wake sheet is appropriate. At the farthest downstream station, the wake travels at speed $Q = 0.97U_0$.

Circulation

The circulation in steady flow is calculated by performing the line integral $\oint u \cdot \mathrm{d}l$ using the steady flow velocity data collected along the control volumes surrounding the test hydrofoil. The time-mean unsteady circulation is also calculated in this manner using the harmonic coefficients of the unsteady velocity data. The steady and time-mean circulation are within 2% of each other; the discrepancy is due to the much coarser spacing of the control volumes in unsteady testing. The time-mean circulation is $\Gamma_0/U_0C = 0.235$.

The unsteady circulation is calculated in three ways to test the assumptions made in each method. First, identification of the general location of unsteady separation allows the calculation of the maximum and minimum possible time-varying circulation. We recall the relation for vorticity flux derived by Sears[20]:

$$-\frac{\mathrm{d}\Gamma}{\mathrm{d}t} = \left(\frac{1}{2}u_e^2 - u_{\text{sep}}\,u_e\right)_A^B \tag{8}$$

where the boundary layer separates at points A and B on the suction and pressure surfaces, respectively. We assume a harmonic form for the circulation as in Eq. (3) and note that the measured edge velocities were found to have negligible harmonic content beyond the fundamental. In addition, the time-mean values of $u_{e,A}$ and $u_{e,B}$ are equal, so that the time dependence of $\Gamma(t)$ is purely harmonic. On the pressure side the separation profile is fixed at the trailing edge: Point B is $x/C = 1.0$ and $u_{\text{sep},B} = 0$. Then the first harmonic equation of Eq. (8) becomes

$$\Gamma_1 \cos(\omega t + \Theta_1) = -(u_{e,0}/\omega)[u_{e1,A}\sin(\omega t + \Theta_A) - u_{\text{sep},A}\sin(\omega t + \Theta_{\text{sep}}) - u_{e1,B}\sin(\omega t + \Theta_B)] \tag{9}$$

The measured edge velocities are given in Table 4. For the unsteady circulation to be pure harmonic, the suction-side separation profile must be at or just downstream of $x/C = 0.97$. Next we assume values for the magnitude and phase of the suction-side separation speed $u_{\text{sep},A}$. The lower bound on the separation speed is

Table 4 Measured unsteady edge velocity

x/C	$u_{e,0}/U_0$	$u_{e,1}/U_0$	Θ_1, deg
	Suction side		
0.90	1.086	0.0284	120.6
0.97	0.968	0.0281	93.04
0.99	0.941	0.0278	83.31
1.00	0.914	0.0261	71.80
	Pressure side		
1.00	0.966	0.0335	198.5

Table 5 Calculated unsteady circulation

Method	Γ_1/Γ_0	Θ_1, deg
Vorticity balance, $u_{sep} = 0$	0.0277	322.1
Vorticity balance, maximum u_{sep}	0.0338	330.8
Linear theory, wake travels at U_0	0.0309	289.3
Linear theory, wake travels at $0.97\,U_0$	0.0300	281.8
Control volume	0.0303	285.1

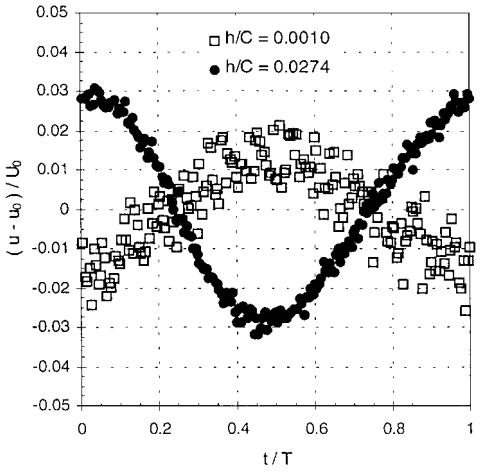

Fig. 9 Unsteady tangential velocity at suction side $x/C = 0.97$.

zero; that is, the separation point is fixed at the surface. The upper bound is the speed measured at the data point closest to the surface at $x/C = 0.97$. These bounds occur because the separation trajectory is located inside this distance from the wall. The magnitude and phase of the unsteady circulation calculated with these assumed separation speeds is then shown in Table 5.

Second, the unsteady circulation is calculated as in classical linear theory: The wake is considered a thin vortex sheet convecting with speed U_0:

$$\gamma\left(x, t + \frac{x - x_{TE}}{U_0}\right) = -\frac{1}{U_0}\frac{d\Gamma}{dt} \tag{10}$$

Using the experimental values of $u^+(x,t)$ and $u^-(x,t)$ from the farthest-downstream measurement station to find $\gamma(x,t)$, the calculated unsteady circulation is shown in Table 5. Also shown is the result for a similar calculation with the wake traveling at speed $0.97\,U_0$, as indicated by the phase speed extracted from the measurements. In either case, the magnitude of the unsteady circulation falls within the bounds given earlier, although the phase difference is quite large: about 50 deg.

Finally, the fundamental harmonic of circulation is found by performing the line integral $\oint u \cdot dl$ using the velocity data collected along the control volume surrounding the test hydrofoil, shown in Table 5. Again, the magnitude falls within the bounds given earlier, although the phase difference is quite large: about 45 deg.

It is thought that the large phase difference between the result of the vorticity balance and the results of the vortex sheet model and the control volume is due to the difficulty in measuring phase when dealing with small-amplitude, noisy unsteadiness. Figure 9 shows the unsteady boundary-layer velocity measured at the closest point to the hydrofoil surface and at the boundary-layer edge, at suction side $x/C = 0.97$. The value of Θ_A is well established, but if the value of Θ_{sep} in Eq. (9) were shifted by $0.1t/T$, which is not unfeasible as seen in Fig. 9, then the phase difference would be less by 15 deg. This uncertainty, along with the uncertainty in knowing the magnitude of the separation speed, suggests that the phase angles calculated using the vortex sheet model and the control volume are less prone to error.

The relative agreement of the values for the magnitude of the unsteady circulation bodes well for the developers of inviscid numerical methods. The time-mean loading can be accurately calculated with an inviscid method if consideration is given to the time-mean location of the separation trajectory, which in the limit of both quasi-steady and very high reduced frequency is the steady separation point.[21] Thus, a steady flow separation criterion, such as that developed by Stratford,[22] can be used for the time-mean problem. Following this, methods that linearize around the correct time-mean solution would be acceptable for prediction of the magnitude of the unsteady lift, though not as reliable for the prediction of phase and unsteady moment. An appropriate unsteady Kutta condition for such a method would be to assume that the shed vorticity in the free shear layers emanating from the time-mean separation points convects at freestream velocity.

Unsteady Loading

The lift and drag in steady flow are calculated using the integral form of Newton's law:

$$\rho \oint \boldsymbol{q}(\boldsymbol{q}\cdot\boldsymbol{n})\,dS + \oint p\boldsymbol{n}\,dS = -D\boldsymbol{i} - L\boldsymbol{k} \tag{11}$$

using the velocity data collected along the control volumes surrounding the test hydrofoil. Note that the integral of shear stress has been neglected. The integral of pressure is written in terms of velocities using Bernoulli's equation, taking care in the wake region where Bernoulli's equation is not strictly valid. Because the downstream leg of the control volume is quite close to the hydrofoil trailing edge, the drag calculated in this manner tends to be overpredicted. A full description of the method is given by Kinnas.[23]

The steady force coefficients generated on the test hydrofoil are $C_L = 0.4702$ and $C_D = 0.01073$. The unsteady lift coefficient is also calculated in the manner already described using the harmonic coefficients of the velocity data: $C_{L1}(t) = 0.01387\sin(\omega t + 274.8\text{ deg})$. By rewriting the inflow, Eq. (2), with phase referenced to the leading edge of the test hydrofoil,

$$w_1/U_0 = (w_1/U_0)\sin(\omega t + 27.74\text{ deg})$$
$$\text{at} \qquad x = 0, \quad z = 0.033C \tag{12}$$

we see that the vertical velocity lags the lift by 247 deg. Even though the separation region is small, the measured lift is much reduced and phase shifted from the result given by the classical theory of Sears,[24] $C_{L1} = 0.02900\sin(\omega t + 344.7\text{ deg})$.

Conclusions

A series of detailed measurements has been made of the velocities in the boundary layer and near wake of a hydrofoil subject to transverse gust loading. The unsteady boundary-layer and near-wake velocities exhibit striking variations of magnitude and phase with height from the surface. As the trailing edge is approached on the suction side, the boundary layer develops two distinct regions across which the fundamental harmonic of velocity has a local amplitude minimum and very large phase shift. In the wake, the local amplitude minima from both suction- and pressure-side boundary layers are mixed out within 20% chord downstream, although large phase shifts are still evident across the shear layer. Despite strong transverse variations in velocity amplitude and phase, the classical representation of the wake as a thin vortex sheet still holds.

Identification of the general location of the boundary-layer separation trajectory has allowed calculation of the unsteady circulation. Comparison with calculations using linear theory indicates that, despite the complicated nature of the shear layers, reasonable predictions of fluctuating lift can be expected if linearizations are made with respect to the correct time-mean solution. Thus, an appropriate

unsteady Kutta condition would be to assume that the shed vorticity in the free shear layers emanating from the time-mean separation points convect at freestream velocity.

Acknowledgments

This research was supported under Office of Naval Research (ONR) Contract N00014-89-J-3194, James A. Fein, Project Manager, and ONR Grant N00014-93-1-1043. The first author's studies at the Massachusetts Institute of Technology were funded in part by the ONR Graduate Fellowship Program. The authors would like to thank Charles Mazel for his tireless efforts in developing and assisting the experiment and B. Matthew Knapp and William Ramsey for their assistance in performing the experiment. E. E. Covert has contributed substantially to this work by his support and criticisms.

References

[1]Ho, Y.-H., and Lakshminarayana, B., "Computation of Unsteady Flowfield over a Hydrofoil, Including Boundary Layer and Wake," *AIAA Journal*, Vol. 35, No. 1, 1997, pp. 40–50.

[2]Paterson, E., and Stern, F., "Computation of Unsteady Viscous Marine-Propulsor Blade Flows—Part 1: Validation and Analysis," *Journal of Fluids Engineering*, Vol. 119, No. 1, 1997, pp. 145–154.

[3]Taylor, L., Busby, J., Jiang, M., Arabshahi, A., Sreenivas, K., and Whitfield, D., "Time Accurate Incompressible Navier–Stokes Simulation of the Flapping Foil Experiment," *Proceedings of the Sixth International Conference on Numerical Ship Hydrodynamics*, Office of Naval Research, Iowa City, IA, 1993, pp. 721–738.

[4]Ho, C., and Chen, S., "Unsteady Kutta Condition of a Plunging Airfoil," *Unsteady Turbulent Shear Flows*, Springer–Verlag, Berlin, 1981, pp. 197–206.

[5]Poling, D., and Telionis, D., "The Response of Airfoils to Periodic Disturbances: The Unsteady Kutta Condition," *AIAA Journal*, Vol. 24, No. 2, 1986, pp. 193–199.

[6]Poling, D., and Telionis, D., "The Trailing Edge of a Pitching Airfoil at High Reduced Frequencies," *Journal of Fluids Engineering*, Vol. 109, No. 12, 1987, pp. 410–414.

[7]Liu, X., Wo, A., and Covert, E., "Unsteady Streamlines near the Trailing Edge of NACA 0012 Airfoil at Reynolds Number of 125,000," *AIAA Journal*, Vol. 28, No. 1, 1990, pp. 169, 170.

[8]Lurie, E., "Investigation of High Reduced Frequency, Separated Trailing Edge Flows," Sc.D. Thesis, Dept. of Ocean Engineering, Massachusetts Inst. of Technology, Cambridge, MA, Sept. 1996.

[9]Commerford, G., and Carta, F., "Unsteady Aerodynamic Response of a Two-Dimensional Airfoil at High Reduced Frequency," *AIAA Journal*, Vol. 12, No. 1, 1974, pp. 43–48.

[10]Satyanarayana, B., and Davis, S., "Experimental Studies of Unsteady Trailing-Edge Conditions," *AIAA Journal*, Vol. 16, No. 2, 1978, pp. 125–129.

[11]Fleeter, A., "Trailing Edge Conditions for Unsteady Flows at High Reduced Frequency," *AIAA Journal*, Vol. 18, No. 5, 1980, pp. 497–503.

[12]Lorber, P., and Covert, E., "Unsteady Airfoil Pressures Produced by Periodic Aerodynamic Interference," *AIAA Journal*, Vol. 20, No. 9, 1982, pp. 1153–1159.

[13]Rice, J., "Investigation of a Two-Dimensional Hydrofoil in Steady and Unsteady Flows," S.M. Thesis, Dept. of Ocean Engineering, Massachusetts Inst. of Technology, Cambridge, MA, June 1991.

[14]Delpero, P., "Investigation of Flows Around a Two-Dimensional Hydrofoil Subject to High Reduced Frequency Gust Loading," S.M. Thesis, Dept. of Ocean Engineering, Massachusetts Inst. of Technology, Cambridge, MA, Feb. 1992.

[15]"Measurement Uncertainty," ANSI/ASME PTC 19.1-1985, Pt. 1, American Society of Mechanical Engineers, New York, 1986.

[16]Lurie, E., "A Note on the Error Analysis of the Flapping Foil Experiment," Dept. of Ocean Engineering, TR 95-3, Massachusetts Inst. of Technology, Cambridge, MA, May 1995.

[17]Patel, M. H., "On Turbulent Boundary Layers in Oscillatory Flow," *Proceedings of the Royal Society of London, Series A: Mathematical and Physical Sciences*, Vol. 353, 1977, pp. 121–144.

[18]Kenison, R., "An Experimental Study of the Effect of Oscillating Flow on the Separation Region in a Turbulent Boundary Layer," AGARD CP-227, Paper 20, Feb. 1978.

[19]Telionis, D., *Viscous Fluid Flow*, Springer–Verlag, New York, 1981, p. 282.

[20]Sears, W., "Some Recent Developments in Airfoil Theory," *Journal of the Aeronautical Sciences*, Vol. 23, No. 5, 1956, pp. 490–499.

[21]Gioulekas, A., "An Alternative to the Kutta Condition for High Frequency, Separated Flows," Ph.D. Thesis, Dept. of Aeronautics and Astronautics, Massachusetts Inst. of Technology, Cambridge, MA, May 1992.

[22]Stratford, B., "The Prediction of Separation of the Turbulent Boundary Layer," *Journal of Fluid Mechanics*, Vol. 5, 1959, pp. 1–16.

[23]Kinnas, S., "Hydrofoil Lift and Drag from Momentum Integrations," Dept. of Ocean Engineering, TR 91-4, Massachusetts Inst. of Technology, Cambridge, MA, Nov. 1991.

[24]Sears, W., "Some Aspects of Non-Stationary Airfoil Theory and Its Practical Applications," *Journal of the Aeronautical Sciences*, Vol. 8, No. 3, 1941, pp. 104–108.

W. Oberkampf
Associate Editor